

The Hawaii Trails Project: Comet-Hunting in the Main Asteroid Belt [★]

Henry H. Hsieh^{1,2}

¹ Astrophysics Research Centre, Queen's University, Belfast, BT7 1NN, United Kingdom
e-mail: h.hsieh@qub.ac.uk

² Institute for Astronomy, University of Hawaii, 2680 Woodlawn Drive, Honolulu, HI 96822,
USA

Submitted 2009 April 16; Accepted 2009 July 30

ABSTRACT

Context. The mysterious solar system object 133P/(7968) Elst-Pizarro is dynamically asteroidal, yet displays recurrent comet-like dust emission. Two scenarios were hypothesized to explain this unusual behavior: (1) 133P is a classical comet from the outer solar system that has evolved onto a main-belt orbit, or (2) 133P is a dynamically ordinary main-belt asteroid on which subsurface ice has recently been exposed. If (1) is correct, the expected rarity of a dynamical transition onto an asteroidal orbit implies that 133P could be alone in the main belt. In contrast, if (2) is correct, other icy main-belt objects should exist and could also exhibit cometary activity.

Aims. Believing 133P to be a dynamically ordinary, yet icy main-belt asteroid, I set out to test the primary prediction of the hypothesis: that 133P-like objects should be common and could be found by an appropriately designed observational survey.

Methods. I conducted just such a survey — the Hawaii Trails Project — of selected main-belt asteroids in a search for objects displaying cometary activity. Optical observations were made of targets selected from among the Themis, Koronis, and Veritas asteroid families, the Karin asteroid cluster, and low-inclination, kilometer-scale outer-belt asteroids, using the Lulin 1.0 m, Small and Moderate Aperture Research Telescope System (SMARTS) 1.0 m, University of Hawaii 2.2 m, Southern Astrophysical Research (SOAR) 4.1 m, Gemini North 8.1 m, Subaru 8.2 m, and Keck I 10 m telescopes.

Results. I made 657 observations of 599 asteroids, discovering one active object now known as 176P/LINEAR, leading to the identification of the new cometary class of main-belt comets. These results suggest that there could be ~100 currently active main-belt comets among low-inclination, kilometer-scale outer belt asteroids. Physically and statistically, main-belt comet activity is consistent with initiation by meter-sized impactors. The estimated rate of impacts and sizes of resulting active sites, however, imply that 133P-sized bodies should become significantly devolatilized over Gyr timescales, suggesting that 133P, and possibly the other MBCs as well, could be secondary, or even multigenerational, fragments from recent breakup events.

Key words. comets: general - comets: individual: 133P/Elst-Pizarro - comets: individual: 176P/LINEAR - minor planets, asteroids - solar system: general

1. Introduction

1.1. Motivation

Comet 133P/(7968) Elst-Pizarro (hereafter 133P), an apparent Themis asteroid family member, has an asteroid-like Tisserand invariant of $T_J = 3.16$ and orbits in the outer main asteroid belt. Its cometary nature was first revealed on 1996 August 7 when a linear dust feature was observed trailing the object (Elst *et al.*, 1996). This dust trail was found to be narrow, structureless, and over 3 arcmin in length. No coma was observed around the nucleus. Previous images from 1979 and 1985 (Marsden, 1996; McNaught *et al.*, 1996) and follow-up observations by Offutt *et al.* (1997) revealed a completely point-source-like nucleus with no apparent dust trail.

The uniqueness of 133P’s dust emission — no other asteroid had ever been seen exhibiting such behavior, and even 133P only demonstrated such behavior once — made it difficult to ascertain its true nature. Some believed the emission to be impact ejecta from a collision between 133P and another asteroid or group of asteroids (*e.g.*, Tóth, 2000), while others believed it to be the result of the sublimation of volatile ices on 133P’s surface (*e.g.*, Boehnhardt *et al.*, 1998). Impact scenarios were unable to plausibly explain the months-long duration of the dust emission episode (Boehnhardt *et al.*, 1996), however, while sublimation required the apparently implausible scenario of surface ice surviving to the present-day on a main-belt asteroid in quantities sufficient for driving cometary activity.

New insight was gained into 133P’s nature when observations in 2002 revealed the return of long-lived dust emission (Hsieh *et al.*, 2004). Given the implausibility of impacts causing prolonged dust emission episodes on the same asteroid in the span of six years, these observations effectively ruled out hypotheses in which impacts were the sole cause of the observed dust emission. After considering other possible emission mechanisms and ruling out each in turn, Hsieh *et al.* concluded that 133P’s dust ejection was most likely driven by the sublimation of volatile material, presumed to be water ice.

This conclusion implied either that (1) 133P was a “lost comet”, *i.e.*, an object originally from the outer solar system that had evolved onto its current orbit via planetary encounters, dynamical resonances, or the non-gravitational influence of asymmetric cometary mass loss, or (2) 133P was an “icy asteroid”, *i.e.*, a dynamically ordinary, native member of the asteroid belt on which preserved, buried ice had been recently exposed, perhaps excavated by an impact. If the “lost comet” hypothesis was correct, the low likelihood of a comet undergoing a dynamical transition from the outer solar system onto a 133P-like orbit (*e.g.*, Ipatov & Hahn, 1997; Fernández *et al.*, 2002) could

* Some of the data presented herein were obtained at the W. M. Keck Observatory, the Gemini Observatory, Subaru Telescope, National Optical Astronomy Observatory (NOAO) facilities at the Cerro Tololo Inter-American Observatory, and Lulin Observatory. Keck is operated as a scientific partnership among the California Institute of Technology, the University of California, and the National Aeronautics and Space Administration, and was made possible by the generous financial support of the W. M. Keck Foundation. Gemini is operated by the Association of Universities for Research in Astronomy, Inc., under a cooperative agreement with the National Science Foundation (NSF) on behalf of the Gemini partnership. Subaru is operated by the National Astronomical Observatory of Japan. NOAO and Cerro Tololo are operated by the Association of Universities for Research in Astronomy, Inc., under co-operative agreement with the NSF. Lulin is supported and was made possible by the National Science Council of Taiwan, the Ministry of Education of Taiwan, and National Central University.

mean that such objects are rare or even non-existent, and that 133P could be the only object of its kind, as was observed. If the “icy asteroid” hypothesis was correct, 133P would not be expected to be unique. Other main-belt asteroids could also possess subsurface ice that could begin sublimating if exposed by impacts. In this case, 133P’s uniqueness could simply be due to the difficulty of discovering such objects serendipitously. An appropriately targeted search could counter this difficulty (Hsieh & Jewitt, 2006a). Believing that this second hypothesis could be correct, I set out to conduct just such a targeted search. In this paper, I describe the design and results of that survey, the Hawaii Trails Project (HTP).

1.2. Background

Various evidence has been found for past and even present water in main-belt asteroids (*cf.* Hsieh & Jewitt, 2006a, and references within), but this fact has not meant that active dust emission due to the sublimation of water ice is commonly observed. Hsieh & Jewitt discuss a number of possible reasons for this inconsistency. Perhaps simply too few 133P-like objects had been observed sufficiently deeply and sufficiently often. Collisional excavation of subsurface ice reservoirs could occur only rarely. Even when collisions do occur, sublimation may not necessarily follow due to the probable non-uniform distribution of subsurface ice reservoirs, and even the successful triggering of sublimation could result in dust emission that is simply too weak to detect from Earth. Finally, observable dust emission is likely to be intermittent and also have a finite lifetime, limited by either local devolatilization of the active site or mantling (Jewitt, 1996, 2002, and references within), further reducing the probability of its detection.

In addition to the above considerations, there are indications that detectable activated asteroids may occupy a narrow range of sizes. The rate of impact excavations of an asteroid depends on its collisional cross-section: large bodies will be struck, and thus activated, more often than small bodies. Volatile material should also survive longer against solar heating on larger asteroids because it can be buried at greater depths. However, Hsieh *et al.* (2004) found that the low dust ejection velocity ($v_{ej} \sim 1 - 2 \text{ m s}^{-1}$) for 133P was extremely similar to the gravitational escape velocity ($v_{esc} \sim 1.5 \text{ m s}^{-1}$), suggesting comparable dust emission would only be observable on bodies of similar or smaller sizes. Comparable emission on larger bodies would be unable to escape the gravity of those bodies and thus never become observable. This scenario may explain why Ceres is not observed to emit dust, despite indications of surface ice (Lebofsky *et al.*, 1981; Vernazza *et al.*, 2005) and even possible water vapor emission (A’Hearn & Feldman, 1992). Despite providing less insulation from the Sun than larger bodies, smaller bodies are also less effectively heated from within by ^{26}Al (since they radiate that heat away more efficiently). In summary, to exhibit dust emission, it seems that icy asteroids need to be large enough to preserve subsurface ice against solar heating and be struck relatively frequently by impactors, but not so large that weak dust emission cannot escape gravity or ice does not survive early radioactive heating. Such conflicts in size preferences suggests that 133P-like asteroids may be even rarer and more difficult to discover than initial considerations might indicate.

1.3. Survey Design

The distribution of present-day ice in the asteroid belt is not well understood. The so-called snow line refers to the distance from the Sun at which the temperature of the protosolar disk was below the condensation temperature of water, allowing ice to become incorporated into accreting planetesimals. Observations of asteroids suggest that the snow line likely existed ~ 2.5 AU from the Sun (Gradie & Tedesco, 1982; Jones *et al.*, 1990), though theoretical models have suggested it may have been as close as the orbit of Mars (Sasselov & Lecar, 2000; Ciesla & Cuzzi, 2006; Lecar *et al.*, 2006), suggesting objects throughout the asteroid belt could have formed icy. Much of this ice has since undergone thermal processing, producing the hydrated minerals now observed on many main-belt asteroids (see Rivkin *et al.*, 2002). Detections of such minerals decline in the outer belt beyond ~ 3 AU (notably, where 133P is found), suggesting that pristine, unaltered ice could still exist in distant main-belt objects (Jones *et al.*, 1990; Scott & Krot, 2005). This hypothesis suggests that a search for 133P-like icy asteroids would be best served by focusing on objects with semi-major axes of $a > 3$ AU, as the HTP does indeed do, although objects with $a < 3$ AU are also considered.

Given the environmental and physical conditions discussed above that are suspected of giving rise to cometary activity in 133P, in the search for objects exhibiting similar activity, the following target categories were considered:

- **Themis family asteroids:** The Themis family is likely the result of the breakup of a parent asteroid about 400 km in diameter ~ 2.5 Gyr ago (Marzari *et al.*, 1995; Tanga *et al.*, 1999; Nesvorný *et al.*, 2003) and is one of the largest and most statistically robust asteroid families known (*e.g.*, Carusi & Valsecchi, 1982; Zappalà *et al.*, 1990). Given their origin from a common parent, Themis family members are thought to be compositionally homogeneous, as corroborated by observational studies showing that the family is dominated by primitive C-type asteroids that also exhibit signs of aqueous alteration (Bell, 1989; Florczak *et al.*, 1999; Ivezić *et al.*, 2002; Mothé-Diniz *et al.*, 2005). The family is also characterized by a high rate of collisions relative to the general main-belt population (Farinella & Davis, 1992; Dell’Oro *et al.*, 2001). Given 133P’s dynamical and possible compositional similarity to Themis family members and the high frequency of collisions within the family, the Themis family was judged to be a natural place to look for 133P-like asteroids. Target objects were selected by conducting a hierarchical clustering analysis (Zappalà *et al.*, 1990, 1994) on proper elements obtained from the AstDys website (<http://hamilton.dm.unipi.it/astdys/>; Knežević & Milani, 2003) and using a cutoff value of $\delta v' = 70 \text{ m s}^{-1}$ with respect to (24) Themis.
- **Low-inclination outer-belt asteroids:** The identification of the main-belt comet (MBC) class (Hsieh & Jewitt, 2006b) during the course of the HTP led to a re-evaluation of the survey’s target selection criteria. In particular, the semimajor axis and inclination of MBC P/2005 U1 (Read) (hereafter P/Read) closely matched those of the Themis family, but its eccentricity did not. This discovery led to the hypothesis that 133P’s low-inclination, and not necessarily its specific association with the Themis family, could be primarily responsible for its activity. Collision rates are in fact known to be enhanced at low inclinations (Farinella & Davis, 1992). Targets were selected by applying limits ($3.0 \text{ AU} < a < 3.3 \text{ AU}$, $e < 0.3$, and $i < 3.0^\circ$) on osculating orbital elements obtained online from Lowell Observatory

(ftp://ftp.lowell.edu/pub/elgb/astorb.dat), permitting the inclusion of even recently discovered asteroids for which proper elements were not yet known. Limits were chosen to span the orbital element distribution of the first three known MBCs, and in fact, also completely encompasses the Themis family.

- **Koronis family asteroids:** As another populous main-belt asteroid family characterized by high collisions rates (Farinella & Davis, 1992), the Koronis family was judged to be another plausible place to look for 133P analogs. Like the Themis family, the Koronis family is the result of the catastrophic disruption of a large parent body ~ 2 Gyr ago (Binzel, 1988; Marzari *et al.*, 1995). Unlike the Themis family, however, the Koronis family is dominated by S-type asteroids (Bell, 1989; Binzel *et al.*, 1993; Mothé-Diniz *et al.*, 2005), which along with their meteoritic analogs, the ordinary chondrites, do not exhibit spectroscopic evidence of significant aqueous alteration (*e.g.*, Rivkin *et al.*, 2002). Nonetheless, due to the high collision rates within this family and the possibility that these asteroids may not actually be completely anhydrous (Grossman *et al.*, 2000; Keil, 2000), Koronis family asteroids were still judged to be viable 133P-analog candidates. Koronis family targets were selected by a hierarchical clustering analysis, using a cutoff value of $\delta v' = 50 \text{ m s}^{-1}$ with respect to (158) Koronis.
- **Karin cluster asteroids:** The Karin cluster is contained within the Koronis family and is likely the result of a recent fragmentation event ~ 5.8 Myr ago (Nesvorný *et al.*, 2002, 2006). Spectroscopic studies have since affirmed both the compositional homogeneity and the young age of the cluster (Sasaki *et al.*, 2004; Brunetto *et al.*, 2006; Vernazza *et al.*, 2006). In the context of this survey, the Karin cluster was interesting because if its parent body only recently broke apart, ice that had been preserved deep inside could suddenly be located at a much shallower depths on the resulting fragments. Even relatively weak subsequent impacts could then easily initiate sublimation. Like the rest of the Koronis family, however, the Karin cluster is dominated by S-type asteroids and so is not an ideal sample from a mineralogical point of view for searching for sublimation-driven dust emission. Given the likelihood of particularly young surfaces, though, these objects were judged to be worthy of at least cursory attention. Karin cluster targets were selected by a hierarchical clustering analysis, using a cutoff value of $\delta v' = 10 \text{ m s}^{-1}$ with respect to (832) Karin.
- **Veritas family asteroids:** Like the Karin cluster, the Veritas family, first identified by Zappalà *et al.* (1995), is likely the result of a recent breakup in the asteroid belt, perhaps just ~ 8.5 Myr ago (Nesvorný *et al.*, 2003; Tsiganis *et al.*, 2007). Intriguingly, such a breakup corresponds with a spike in ^3He concentrations found in sea-floor sediment records from that time period (Farley *et al.*, 2006). The young age of the Veritas family made it interesting for this survey for the same reasons as the Karin cluster. Unlike the Karin cluster, however, the Veritas family appears to be dominated by C-type asteroids (Mothé-Diniz *et al.*, 2005), the same type of asteroids that dominate the Themis family, making it a particularly promising place to search for 133P analogs. Veritas family targets were selected by a hierarchical clustering analysis, using a cutoff value of $\delta v' = 40 \text{ m s}^{-1}$ with respect to (490) Veritas.

Targets from these categories were selected for each observing run based on visibility, expected visual magnitude ($18 \lesssim m_R \lesssim 20$ mag targets for UH 2.2 m runs, brighter targets for smaller telescopes or in non-photometric conditions, and fainter targets for larger telescopes), distance from

the moon, and distance from the galactic plane. I also sought to observe asteroids matching 133P closely in physical size (as parameterized by absolute magnitude, H_V), or approximately kilometer-scale, given the issues discussed in §1.2. The aim was to achieve moderately deep imaging for as many asteroids as possible. As such, exposure times were selected such that signal-to-noise ratios of at least $S/N = 20$ for 93.5% (614 out of 657) of the surveyed targets, and at least $S/N = 10$ for 99.2% (652 out of 657) of the surveyed targets were reached.

While most observations were made of unique asteroids, repeat observations of individual asteroids were not expressly avoided. Given the expected transient nature of any cometary activity, continued monitoring of comet candidates is in fact, in principle, vital to fully characterizing their active natures. In a larger survey, all objects would have been observed multiple times, but for the relatively small-scale HTP, repeat observations were made only occasionally.

2. Observations

Several ground-based optical observatories were used to conduct this survey: the University of Hawaii (UH) 2.2 meter telescope, the 8.1 m Gemini North Observatory, the 8.2 m Subaru telescope, and the 10 m Keck I Observatory on Mauna Kea in Hawaii, the 1.0 m telescope operated by the Small and Moderate Aperture Research Telescope System (SMARTS) consortium at the Cerro Tololo Inter-American Observatory (CTIO) and Cerro Pachon's 4.1 m Southern Astrophysical Research (SOAR) telescope in Chile, and the Lulin 1.0 m telescope in Taiwan (Table 1). Data was obtained on 88 separate nights (Table 2).

Either a Tektronix 2048×2048 pixel charge-coupled device (CCD) or the Orthogonal Parallel Transfer Imaging Camera (OPTIC) was used at the f/10 focus of the UH 2.2 m telescope. Other instruments used on Mauna Kea telescopes were the Gemini Multi-Object Spectrograph (GMOS) (Hook *et al.*, 2004) in imaging mode on Gemini, the Subaru Prime Focus Camera (Suprime-Cam) (Miyazaki *et al.*, 2002) on Subaru, and the Low-Resolution Imaging Spectrometer (LRIS) (Oke *et al.*, 1995) on Keck. Observations using the CTIO 1.0 m telescope employed either an Apogee 512×512 CCD or an STA 4064×4064 CCD (Y4KCam), while observations on the SOAR telescope employed the SOAR Optical Imager (SOI) (Schwarz *et al.*, 2004). Observations using the Lulin 1.0 m telescope were made using a VersArray:1300B CCD (Kinoshita *et al.*, 2005). All observations were obtained through broadband filters approximating the Kron-Cousins *BVRI* photometric system except for observations at Gemini which employed $g'r'i'z'$ broadband filters similar to those used for the Sloan Digital Sky Survey (SDSS). Further telescope details are listed in Table 1.

Standard image preparation (bias subtraction and flat-field reduction) was performed on all data. Flat fields were constructed either from dithered images taken nightly of the twilight sky or images of the illuminated interior of the telescope dome. Photometry on standard stars and target objects was performed by measuring net fluxes contained within circular apertures with optimum sizes determined from curve of growth analysis and dependent on the nightly seeing. The sky background to be subtracted was determined from the median pixel value within a circular annulus surrounding each central aperture. Photometry was calibrated to Landolt (1992) standard stars to produce absolute photometry for the target objects. Photometric uncertainties are estimated to be 0.1 mag for objects observed in photometric conditions and 0.5 mag for objects observed in non-photometric conditions (see Table 2).

3. Analysis and Results

3.1. Activity Assessment

To search for low-level cometary activity, all images for a given target on a single night were aligned on the object's photocenter using linear interpolation and then summed to produce a single composite image. Asteroids with possible cometary activity were identified visually from these composite images, and then the corresponding individual images were inspected to assess the plausibility of the detection (*e.g.*, whether the morphology of a suspected cometary feature matched that expected for comets, whether the feature consistently appeared in each individual image, whether the motion of the feature and object against the background star field were identical, and whether there were any signs that the features could be attributed to scattered light or imperfect flatfielding). After this close inspection, if an object showed credible evidence of being active, confirmation of activity was then attempted using deep follow-up imaging. Observations for which activity was impossible to assess and were therefore unsuitable for analysis (*e.g.* those where the object was strongly affected by scattered light from a nearby bright star, or where poor telescope stability resulted in inconsistent point-spread functions among individual images of the same object) were discarded.

Various systematic, quantitative means of searching for cometary activity in HTP data were considered, including one-dimensional surface brightness profile analysis (*e.g.*, Luu & Jewitt, 1992; Hsieh & Jewitt, 2005), radial surface brightness profile analysis (*e.g.*, Luu & Jewitt, 1990), and trail searching (Hsieh & Jewitt, 2005). One-dimensional surface brightness profile analysis can be useful in that it accounts for trailing of point source templates (*i.e.*, field stars) caused by non-sidereal tracking and long exposure times of each target image. Trailing effects are avoided by measuring the surface brightness profiles of targets and field stars in the direction perpendicular to the apparent motion of the target. This technique is best-suited for detecting coma that extends radially in all directions from an object, or directed emission not aligned with the direction of the object's apparent motion, but would miss directed emission oriented along the direction of an object's apparent motion (as was observed for 133P).

Radial surface brightness profile analysis is sensitive to cometary features extended in any direction, but requires the use of circularly-symmetric point source templates. Field stars from target images were generally unsuitable due to trailing, requiring the use of either standard star images or separately-observed sidereally-tracked target images to obtain reference star templates, but both of these alternatives were problematic as well. Even with the use of tip-tilt guiding, continuous atmospheric fluctuations and small but non-negligible mechanical instabilities in the telescopes used (particularly while tracking non-sidereally) resulted in systematically wider point-spread functions (PSFs) for long-exposure target images than short-exposure standard star images. Those same image quality fluctuations also adversely affected the utility of separate sidereally-tracked target images by making it difficult to distinguish ordinary image-to-image PSF fluctuations from the small deviations that could actually indicate the presence of activity. This technique also averages any dust emission over all radial directions, reducing sensitivity to directed emission.

Searching for dust emission specifically like 133P's dust trail, which could form if an object emits large ($\gtrsim 10 \mu\text{m}$) dust particles at low velocities ($\sim 1 - 2 \text{ m s}^{-1}$) as 133P did (Hsieh *et al.*, 2004), can be done by searching for excess flux above sky background along the object's orbital plane (the expected direction of a trail). This technique is not sensitive to near-nucleus activity,

however, and furthermore, is highly susceptible to contamination from field stars or galaxies due to the large amount of sky that must be examined for evidence of trails.

All three techniques are prone to false detections, which can arise from nearby faint field stars or galaxies masquerading as active features, contamination of sky background samples, imperfect flatfielding, scattered light from nearby bright or saturated field stars, and PSF variability between images or even within the same image (*i.e.*, as a function of position on the CCD). Thus, any automated detection scheme still requires confirmation by visual inspection. Given the focused nature of this survey (targeted deep imaging of single objects), the resulting small sample size (~650 composite images to be evaluated over 3 years), and the significant human intervention needed to supplement any of the quantitative detection algorithms considered, I opted to simply visually inspect each target for evidence of activity. This approach is certainly less feasible for searching for comets in much larger data sets, particularly the ones that will be produced by upcoming survey telescopes like the Panoramic Survey Telescope and Rapid Response System (Pan-STARRS; Hodapp *et al.*, 2004) and the Large Synoptic Survey Telescope (LSST; Jones *et al.*, 2009). For the HTP, however, direct visual inspection was judged to be the most efficient (given the small sample size) and effective method for evaluating the active nature of the targets in this survey.

3.2. Survey Results

In total, 599 unique asteroids were observed as part of the HTP, with 544 asteroids observed once, 52 asteroids observed twice, and 3 asteroids observed three times, totaling 657 separate observations (Table 3). Hereafter, all observations (including those of objects observed multiple times) are considered independent of one another. This approach is taken since it is not known where along their orbits other 133P-like asteroids could exhibit activity, and also since inactivity observed for an asteroid at one time does not necessarily rule out activity at another time.

The numbers of targets observed from each target category are shown in Table 4 and Fig. 1, for which it should be noted that all Themis family members are also counted as low-inclination outer belt asteroids, and all Karin cluster members are also counted as Koronis family members. The Veritas family is independent of all other target categories. Slightly more than half (389 of 657) of observed targets were Themis family members, reflecting the prediction that these were the objects among which other 133P-like asteroids would most likely be found. This histogram, and others following it, also show the relative numbers of targets for which shallow, medium, and deep surface brightness detection limits were reached.

The semimajor axis versus eccentricity distribution and semimajor axis versus inclination distribution of surveyed targets in the context of the background main-belt population are shown in Figs. 2 and 3, respectively. These distributions primarily reflect the family association or orbital element criteria of HTP target categories (§1.3).

3.3. Discovery of the Main-Belt Comets

The most significant result from the HTP was the discovery of cometary activity in asteroid 118401 (1999 RE₇₀; subsequently designated 176P/LINEAR; hereafter 176P), on 2005 November 26 by Gemini North (Hsieh & Jewitt, 2006b; Hsieh *et al.*, 2006). Coincidentally, this discovery was made just a month following the serendipitous discovery of P/Read (Read *et al.*, 2005), another

cometary object orbiting completely within the main asteroid belt, on 2005 October 24 by the 0.9 m Spacewatch telescope. Together, 133P, P/Read, and 176P formed a new class of objects which were dubbed MBCs (Hsieh & Jewitt, 2006b). Following the completion of the HTP, a fourth MBC, P/2008 R1 (Garradd) (hereafter, P/Garradd; Garradd *et al.*, 2008), was discovered on 2008 September 2 by the 0.5-m Uppsala Schmidt telescope at Siding Spring. The properties of the currently-known MBCs are listed in Table 5. All other HTP observations (including a previous observation of 176P using the Lulin 1.0 m telescope one month prior to the discovery of the object’s cometary nature by Gemini) were judged to show no evidence of cometary activity.

The extremely limited data set used to discover the currently-known population (three members were discovered serendipitously by 0.5 m to 1.0 m telescopes, and another was discovered by a targeted survey composed of only 657 asteroid observations) implies that a much larger undiscovered population exists. The existence of multiple known MBCs and the implication of a much larger as-yet undiscovered population runs counter to the prediction made by the “lost comet” hypothesis that 133P should be alone in the main belt, making the “icy asteroid” hypothesis, which predicts that such objects should be widespread in the main belt, much more likely (§1.1).

4. Discussion

4.1. Selection Effects and Biases

It should be emphasized that the HTP was not designed as a random sampling of the main asteroid belt and cannot be interpreted as such. On the contrary, it was designed to maximize the probability of discovering 133P-like asteroids and so employed very specific physical and dynamical target selection criteria. The HTP was also subject to a number of ordinary observational biases.

Histograms showing the distributions of various physical and dynamical properties and observational circumstances for surveyed targets are shown in Figs. 4 and 5. For reference, the locations of the known MBCs (for Fig. 4) or the range of locations of the known MBCs while they were observed to be active (for Fig. 5) in these distributions are marked. These histograms reflect the following intentional selection effects or observational biases:

- The distributions of semimajor axes (Fig. 4a), eccentricities (Fig. 4b), and inclinations (Fig. 4c) of surveyed targets strongly reflect the focus on specific asteroid families, particularly the low-inclination, moderate eccentricity Themis family at $\sim 3.1 - 3.2$ AU and the low-inclination, low-eccentricity Koronis family at ~ 2.9 AU (also see Figs. 2 and 3).
- The distribution of absolute magnitudes (Fig. 4d) of surveyed targets reflects the focus on asteroids similar to 133P ($H_V = 15.9$ mag; Hsieh *et al.*, 2009a). It is also affected, however, by the fact that smaller targets are fainter and are more difficult to image to the same depth as larger, brighter targets. The known population of small objects is also quite incomplete, again due to the faintness of these objects and the difficulty of discovering them. Larger asteroids were furthermore more likely to have well-known orbits and calculated proper orbital elements, necessary for computing family linkages on which initial target selection relied.
- The increased difficulty of observing fainter objects farther from perihelion ($\nu = 0^\circ$) meant that fewer were observed, as can be seen from the heliocentric distance and true anomaly distributions of HTP observations (Figs. 5a and 5b). The resulting oversampling of near-perihelion objects means that even if the seasonal activity modulation hypothesis discussed above (§1.2) is

correct and there is an equal likelihood of activity along an asteroid's entire orbit, active objects are still more likely to be near perihelion when they are observed. For this reason, the discovery of near-perihelion activity in this survey should not be interpreted as confirmation that activity in 133P-like asteroids is correlated to perihelion passages. Similarly, the correlation of activity of serendipitously discovered MBCs to perihelion passages should not necessarily be interpreted as real either since this correlation may simply be due to the fact that the objects are closer to observers near perihelion and their activity is therefore brighter and more easily detected.

- The low inclinations of most targets (Fig. 4c) necessarily meant that they were also observed at low orbit plane angles (Fig. 5c). This trend is significant because low orbit plane angles are where dust emission is most easily observed. When dispersed by solar radiation pressure, emitted dust will tend to spread out in a plane behind an object and aligned with its orbit. Thus, when the Earth is also aligned with the object's orbit plane, the optical depth of the emitted dust is maximized. Indeed, when observed to be actively emitting dust, the first three known MBCs were at low orbit plane angles with respect to the Earth ($|\alpha_{pl}| < 0.6^\circ$).
- The distribution of apparent magnitudes (Fig. 5d) primarily reflects the fact that the majority of HTP observations were made using the UH 2.2 m telescope and objects with visual R -band magnitudes of $18 \lesssim m_R \lesssim 20$ mag were judged to be the most effectively and efficiently observed with that telescope aperture. Fainter asteroids were observed with larger telescopes such as Subaru, Gemini, and Keck I, but these targets typically were not imaged as deeply as brighter objects due to the desire to also observe as many of these smaller asteroids as possible.

It should be noted that P/Read was serendipitously discovered and so its strong orbital similarities to 133P and 176P cannot be easily explained by selection effects or observational biases. Its discovery may in fact indicate a true predisposition of the region near the Themis family for harboring MBCs. It should also be noted, however, that the discovery of P/Garradd in a completely unexpected, and unsurveyed, region of the main belt underscores the point that the HTP cannot and should not be viewed as a representative sampling of the cometary content of the entire main belt.

Since the discovery of 176P's cometary nature as part of the targeted HTP, at least two untargeted surveys have been conducted to search for other MBCs. Gilbert & Wiegert (2009) searched 12390 main-belt objects observed as part of the Very Wide segment of the Canada-France-Hawaii Telescope (CFHT) Legacy Survey, finding one known comet (active Centaur 166P/NEAT) and one unknown comet with an unknown orbit, but no active objects with confirmed main-belt orbits. For a small portion of their survey (952 targets), automated techniques, some similar to those considered for the HTP, were used to search for cometary activity. As in the HTP, though, the majority of their targets (11438 targets) were simply assessed visually. Both cometary objects were found by visual inspection. From these results, they estimated an upper limit of ~ 800 weakly active MBCs among objects larger than 1.5 km in diameter with semimajor axes between 3.0 AU and 5.0 AU, consistent with the results found by the HTP (§4.3). Meanwhile, Sonnett *et al.* (2008) searched 1850 objects observed with the CFHT as part of the Thousand Asteroid Light Curve Survey (Masiero *et al.*, 2009). Several different automated techniques were employed to search for activity, but ultimately no evidence of activity was found in any of those objects.

Such untargeted surveys are clearly better suited than the HTP for developing generalizations about the prevalence of MBCs throughout the asteroid belt in that they do not focus on specific regions of orbital parameter space. The correlated disadvantage of the untargeted approach, however, that the probability of discovering MBCs is much lower than that of targeted surveys like the HTP, as is reflected by the lack of detections in either untargeted survey, despite both having much larger target sample sizes than the HTP.

4.2. Survey Sensitivity

The image depth to which candidate objects should be observed was a key uncertainty at the start of this survey. When an active 133P was observed on 2002 November 5, the surface brightness of a representative section of the trail (just outside the seeing disk of the nucleus) was $\Sigma = 25.2 \text{ mag arcsec}^{-2}$. In previous observing runs that fall, 133P's trail was brighter. Thus, its 2002 November 5 surface brightness could be considered a minimum surface brightness sensitivity for future observations searching for similar activity. This need for deep imaging had to be balanced with maximizing the target sample size to maximize the likelihood of finding an object that was actually active. In the end, $\sim 75\%$ (488) of the 657 observations made had 3σ surface brightness detection limits of $\Sigma_{lim} = 25.2 \text{ mag arcsec}^{-2}$ or better, though many observations went even deeper, with more than 25% (170 objects) having 3σ surface brightness detection limits of $\Sigma_{lim} > 26.0 \text{ mag arcsec}^{-2}$ (Table 3).

The discovery of 176P's cometary nature during this survey was made with two 120 s exposures (which, stacked together, had a 3σ surface brightness detection limit of $\Sigma_{lim} = 26.8 \text{ mag arcsec}^{-2}$) on 2005 November 26 on the 8 m Gemini telescope. In these observations, the tail had a typical surface brightness of $\Sigma = 25.3 \text{ mag arcsec}^{-2}$, a surface brightness which should have been detectable by $\sim 70\%$ (466) of HTP observations. One cautionary note is that 176P was also observed on 2005 October 24 using the Lulin 1.0 m telescope just one month before the discovery of its cometary activity by Gemini on 2005 November 26. No activity was detected in the Lulin data, which had a surface brightness detection limit of $\Sigma_{lim} = 25.3 \text{ mag arcsec}^{-2}$, indicating that 176P's tail could simply have been fainter then, or perhaps poor seeing ($\sim 1''.5$ for the Lulin data, compared to $\sim 0''.9$ for the Gemini data) could be to blame for the lack of observed activity. Only $\sim 75\%$ (484) of HTP observations were made on nights when the seeing was $\leq 1''.1$, and of these observations, 427 (65% of the total survey) had $\Sigma_{lim} > 25.3 \text{ mag arcsec}^{-2}$.

To provide a physical basis of comparison, the ratio of dust surface area to the total nucleus scattering cross-section, C_d/C_n , contained within $1 \times 10^6 \text{ km}$ at the geocentric distance of each target object, that is represented by Σ_{lim} is also calculated and shown in Table 3. This parameter is roughly correlated with S/N and is computed to relate the activity detection limit of an observation (which is largely dependent on the total effective exposure time, size of telescope used, and proximity of the Moon or bright stars, but not the target itself) to the size and brightness of the target being observed. For reference, $C_d/C_n = 0.0039$ for 133P's trail when observed by the UH 2.2 m telescope on 2002 November 5, while $C_d/C_n = 0.0022$ for 176P's tail when observed by Gemini on 2005 November 26. Thus, activity as intense as 176P's activity, relative to the size and brightness of the nucleus, should have been detectable in $\sim 70\%$ of HTP observations (where 466 of 657 observations had surface brightness detection limits equivalent to $C_d/C_n \leq 0.022$), while activity as intense as

133P's activity, relative to its nucleus, should have been detectable in $\sim 90\%$ (588 of 657) of HTP observations.

4.3. MBC Population Size

A natural question to ask following the completion of the HTP is how many other active MBCs are implied to exist? This question is rather tricky to answer given the various ways that HTP results can be scaled to the general main-belt population and the difficulty of interpreting the statistical implications of a single detection. To start out, however, the probability, P_{actv} , that a randomly selected object in a given population will be active at a given time can be estimated by

$$P_{actv} = \frac{n_{actv}}{n_{tot}} \cdot f_{orb} \quad (1)$$

where n_{actv} is the number of active objects in the population, n_{tot} is the total number of objects in the population, and f_{orb} is the fraction of an object's orbit during which it is actually active. For this analysis, I adopt the active orbit fraction of 133P of $f_{orb} \approx 0.25$ (Hsieh *et al.*, 2004, and references within) to be typical of all MBCs.

Observationally, P_{actv} can be estimated from

$$P_{actv} = \frac{n_{det}}{n_{surv}} \quad (2)$$

where n_{det} is the number of detections of activity in a particular sample set, and n_{surv} is the total number of candidate objects observed that belong to that sample set. Thus, combining Equations 1 and 2, one obtains

$$n_{actv} = \frac{n_{det}n_{tot}}{n_{surv}f_{orb}} \quad (3)$$

The HTP detected one active MBC ($n_{det} = 1$), with the survey size ranging from $n_{surv} = 657$, if all surveyed objects are included, to $n_{surv} = 427$, if only observations judged to be sufficiently sensitive and made in sufficiently good seeing conditions to have permitted the detection of 176P-like activity (§4.2) are considered. Hereafter, only the latter group of objects, where $n_{surv} = 427$, is considered.

As of 2009 April 1, there are approximately 450,000 known main-belt asteroids. If the entire asteroid belt is considered to be the candidate population and using $f_{orb} \approx 0.25$ (assuming 133P to be typical of all MBCs), Equation 3 indicates that there could be ~ 4200 MBCs in the main belt. This result, however, suggests that all main-belt asteroids are equally likely to be MBCs, which is likely not the case.

Refining this analysis, one might note that, just like 133P, 176P was discovered among the highly collisionally-active, C-type-dominated Themis family, and therefore Themis family targets may be a more appropriate sample from which to scale these results. In this case, $n_{tot} = 2271$ and $n_{surv} = 262$, giving $n_{actv} \sim 35$. Like scaling to the entire main-belt population, this calculation assumes that all Themis family members are equally likely to display activity. As before, however, this is likely not the case (§1.2): small asteroids are more likely to display observable evidence of sublimation due to their small escape velocities and higher likelihood of being recently collisionally-produced fragments (Cheng, 2004) that may have near-surface ice deposits. Thus far, this hypothesis is supported by the evidence. All four currently-known MBCs have $H_V > 15$. If only Themis family asteroids in this size range are considered, using $n_{surv}(H_V \geq 15.0) = 205$ and

$n_{tot}(H_V \geq 15.0) = 358$, one finds that there may only be ~ 10 MBCs that are detectable via the type of optical observations that were done in this survey.

Refining this analysis yet again, one might note that unlike 133P and 176P, P/Read has an oscillating eccentricity that places it beyond the approximate bounds of the Themis family. It is possible that when proper elements become available for P/Read, it will in fact be found to be associated with the Themis family. Nonetheless, immediately following P/Read's discovery, I began surveying other asteroids that, like P/Read, matched the Themis family in semimajor axis and inclination, but not in eccentricity. These are the HTP's low-inclination outer-belt targets. Using this sample (which only includes objects with $H_V \geq 14.0$) where $n_{tot} = 8647$ and $n_{surv} = 327$ (the total number of observed low-inclination targets with $H_V \geq 14.0$), I estimate that $n_{actv} \sim 100$ among kilometer-scale, low-inclination, outer-belt asteroids. Using analogous lines of reasoning for the other target categories surveyed as part of the HTP where $n_{det} < 1$ and only targets with $H_V \geq 14.0$ are considered, I estimate that $n_{actv} < 150$ for the Koronis family, $n_{actv} < 40$ for the Karin cluster, and $n_{actv} < 15$ for the Veritas family.

The design of the HTP as a highly biased, targeted survey means that it cannot be used to infer the prevalence of MBCs in the general main belt population. There are large regions of the main belt that were not surveyed (*cf.*, Figs. 2 and 3) and the recent discovery of the fourth-known MBC, P/Garradd, shows that MBCs can certainly exist in those unsurveyed regions (see Fig. 4). Furthermore, preliminary results suggest that the nuclei of P/Read and P/Garradd are both extremely small (sub-kilometer-scale; Hsieh *et al.*, 2009b; Jewitt *et al.*, 2009), suggesting that, if not for their prodigious cometary activity, they would never have been discovered due to their extreme faintness. These results further suggest that more as-yet unknown sub-kilometer-scale cometary asteroids might be discovered in the future, but without better knowledge of the size of the main-belt population at this size scale and a systematic, statistically significant survey of this population, it is difficult to predict how many of these small MBCs there might be.

Jewitt *et al.* (2009) found that while P/Garradd is characterized by an asteroidal $T_J = 3.217$, its orbit is unstable on a timescale of ~ 20 Myr, due largely to the influence of the nearby 8:3 mean-motion resonance (2.706 AU from the Sun) with Jupiter and the ν_6 secular resonance (near 2.1 AU from the Sun). Because of these two facts, they hypothesize that the object may have migrated to its current location from a source region in the outer asteroid belt, perhaps where the other three known MBCs currently reside. This hypothesis is slightly problematic as de Elía & Brunini (2007) have actually found that mixing should be minimal among zones of the main asteroid belt delineated by the strongly chaotic 3:1 (2.5 AU from the Sun), 5:2 (2.8 AU from the Sun), and 2:1 (3.27 AU from the Sun) mean motion resonances with Jupiter. In a study of V-type asteroids in the middle main belt, however, Roig *et al.* (2008) found that a non-negligible number of asteroids could be capable of migrating outward across Jupiter's 3:1 resonance, and thus it is conceivable that P/Garradd could be an icy outer-belt asteroid that analogously migrated inward across Jupiter's 5:2 resonance.

From these results, it is clear that the small number of currently-known MBCs greatly hinders any attempt to estimate just how common they are in the main asteroid belt, and that better constraints may not become available until deep-imaging, all-sky survey telescopes like Pan-STARRS and LSST discover more. This discussion has also focused on currently active MBCs. If these objects are recently activated by collisions, there must also be a large population of icy asteroids that have *not* been recently activated. In the above analysis, all asteroids in a given target category are

assumed to be dormant MBCs, but in truth, the extent of this dormant population is unconstrained, except that it must assuredly be larger than the active population. In fact, if recent thermal models are correct, the population of dormant MBCs could, in principle, span the entire main belt (Fig. 4 in Schorghofer, 2008).

4.4. Impact Circumstances and Environment

Hsieh *et al.* (2004) estimated a peak mass loss rate for 133P in 2002 on the order of $\sim 0.01 \text{ kg s}^{-1}$, corresponding to an effective area of exposed water ice of up to a few hundred square meters (assuming a gas-to-dust ratio of 1), or an active “vent” (assumed here to be circular) with a radius of $r_v \sim 10 \text{ m}$. Assuming that the vent was collisionally produced, this amount of exposed ice requires a crater of that size or larger. The size of the required crater is difficult to constrain as it depends on several factors, such as surface topology and the depth of the subsurface ice. If the layer of inert surface material is thick, volatile material may only become exposed in the deepest portion of the crater. Furthermore, a rapid expected mantling timescale ($\tau_m \sim 15 \text{ days}$ for a $r \sim 2 \text{ km}$ nucleus; Jewitt, 1996, 2002) suggests that much of the ice initially exposed by an activating impact is likely to be quickly reburied by rubble mantle growth, necessitating an initial crater that is larger than the calculated surface area of exposed ice needed to sustain the observed rate of sublimation.

In order to calculate the size of the impactor required to create a reasonably-sized vent on an MBC, assuming that these vents are in fact collisionally-produced, one must first test whether the creation of 133P’s active vent was likely to be gravity-dominated or strength-dominated using

$$R \approx \frac{8G\pi\rho_a^2 r_a r_v}{3Y} \quad (4)$$

where G is the gravitational constant, ρ_a is the asteroid’s mean bulk density (taken here to be $\rho_a = 1300 \text{ kg m}^{-3}$), r_a is the asteroid radius, Y is the strength parameter (taken here to be $Y \sim 5 \times 10^5 \text{ Pa}$, a typical value used for porous silicates), and $R > 1$ for gravity-dominated crater formation and $R < 1$ for strength-dominated crater formation (Davis, 1999). The density used here is a minimum critical density required for 133P to be stable against centrifugal forces induced by its rapid rotation (Hsieh *et al.*, 2004), but is also consistent with the density of $\rho_a = 1300 \pm 300 \text{ kg m}^{-3}$ found for (253) Mathilde (another C-type asteroid) from a flyby by the Near-Earth Asteroid Rendezvous (NEAR) spacecraft (Veveřka *et al.*, 1999). One finds $R \approx 4 \times 10^{-5}$ for the minimum inferred crater size of $r_v \sim 10 \text{ m}$, and $R \approx 7 \times 10^{-2}$ for a crater as large as 133P itself (*i.e.*, $r_v \sim 1.9 \text{ km}$). These results indicate that, due largely to 133P’s extremely low surface gravity, any cratering on the object likely occurs in the strength-dominated regime.

One therefore should use a crater scaling relation for the strength-dominated regime,

$$r_i = \frac{r_v}{C'_D} \left(\frac{6\rho_a}{\pi\rho_i} \right)^{1/3} \left(\frac{\rho_i v_i^2}{Y} \right)^{\beta/(\beta-1)} \quad (5)$$

where r_i is the impactor radius, $\rho_i \sim 2600 \text{ kg m}^{-3}$ is the assumed impactor density, $v_i \sim 5 \text{ km s}^{-1}$ is the assumed impactor velocity, and C'_D and β are material-dependent constants, adopted here to be $C'_D = 1.5$ and $\beta = 0.165$ (O’Brien *et al.*, 2006). One thus finds that an impactor with a radius of at least $r_i \sim 0.6 \text{ m}$ is needed to excavate an active site with a radius of $r_v \sim 10 \text{ m}$. Using this radius as the minimum possible size for the active site, and taking this calculation as an order-of-magnitude estimate, hereafter I adopt $r_i \sim 1 \text{ m}$ as the approximate size of the impactor responsible

for collisionally activating 133P, and furthermore, assume this activating impactor size to also be typical for all other MBCs.

Unfortunately, the population of meter-sized bodies in the asteroid belt is poorly constrained, meaning that impact rates by such small impactors are likewise poorly constrained. Extrapolations of the known main-belt population (which extends down to approximately kilometer-sized bodies), however, indicate that there may be approximately $n_i \sim 10^{13}$ meter-sized bodies in the main belt, where both Cheng (2004) and Bottke *et al.* (2005) find an approximate sub-kilometer main-belt size distribution function of $n_i \sim kr_i^{-2.5}$, where $k = 3.2 \times 10^5$. Approximating the main belt as a cylinder of $r = 3.3$ AU and $h \sim 1.5$ AU (where h is the approximate thickness of the asteroid belt measured perpendicular to the plane of the solar system), with an $r = 2.1$ AU cylindrical hole in its center, and assuming objects are distributed uniformly throughout the main belt, one derives an approximate impactor number density of $N_i \sim 10^{-22} \text{ m}^{-3}$.

Then, using

$$\tau_i \sim (v_{rel}\pi r_a^2 N_i)^{-1} \quad (6)$$

for 133P with an effective radius of $r_a = 1.9$ km and having typical relative encounter velocities of $v_{rel} \sim 5 \text{ km s}^{-1}$ with other main belt objects (*e.g.*, Farinella & Davis, 1992), one obtains an approximate impact time scale per object of $\tau_i \sim 2 \times 10^{11}$ s, or about one impact by a meter-sized projectile every 6000 yr (~ 1000 orbits). This should be regarded as an order-of-magnitude estimate only, as it is based on an assumption of uniform impactor density throughout the main belt (certainly untrue), which in turn is based on an extrapolation of the main-belt size-frequency distribution. For reference, following analogous lines of reasoning, order-of-magnitude timescales for impacts by 0.1-meter-sized and 10-meter-sized projectiles are $\tau_i \sim 10$ yr (~ 2 orbits) and $\tau_i \sim 1$ Myr ($\sim 2 \times 10^5$ orbits), respectively.

4.5. Active Lifetimes

Like typical crater and impactor sizes for the MBCs, the typical lifetime of an active vent is difficult to constrain and is likely highly variable for individual situations. This is in fact the case for all comets (*cf.* Sekanina, 1990), as numerous variables (*e.g.*, location and depth of the activating crater, local ice content, local surface topography, orbital obliquity, perihelion distance, nucleus rotation rate) affect a particular vent's lifetime. Clearly a vent's active lifetime depends on the area of ice exposed, the size and morphology of the underlying volatile reservoir, and the depth of penetration of the activating impact. Surface topography near the active site and orbital parameters will affect the amount of solar radiation received, affecting the intensity and duration of sublimation activity. In the case of 133P, which has a rotation period of 3.471 hr (Hsieh *et al.*, 2004), centrifugal forces induced by rapid rotation could affect a vent's active lifetime by inhibiting rubble mantle growth, slowing this means of cometary deactivation.

As directly calculating the lifetimes of active sites on MBCs is difficult to do with any confidence, an order-of-magnitude estimate can instead be derived from the statistics of the HTP survey itself. Earlier (§4.3), it was estimated that 100 of the 8647 kilometer-scale, low-inclination, outer belt asteroids known at the time when the HTP was in progress could be currently active. Making the simplifying assumption that all asteroids in that population are equally likely to become active over their lifetimes, one finds that, on average, each individual asteroid is active over $f_{tot} \sim 0.01$

of its total lifetime. However, 133P is currently observed to be active over $f_{orb} \sim 0.25$ of its orbit. Thus, assuming 133P to be typical of all kilometer-scale, low-inclination, outer belt asteroids and if an activating collision occurs every ~ 1000 orbits, as estimated above, then the activity initiated by each collision should persist for ~ 40 orbits, or about 250 yr.

For MBCs with active orbit fractions of $f_{orb} = 0.1$ or $f_{orb} = 0.5$, activity would instead be expected to persist for 600 yr and 120 yr, respectively. Additionally, if HTP survey statistics are incorrect by a factor of 2 (due, for example, to the extremely small-number statistics associated with a single detection, the uneven sensitivity of HTP observations, or other factors), the derived active vent lifetime could vary from 60 yr (using $f_{tot} = 0.005$ and $f_{orb} = 0.5$) to 1200 yr (using $f_{tot} = 0.02$ and $f_{orb} = 0.1$). The typical lifetime of an active vent can therefore be estimated to be $\tau_{actv} \sim 10^2 - 10^3$ yr.

If it is instead assumed that MBC activity is caused by 0.1-meter-sized impactors, the higher impact rate of these more populous impactors implies $\tau_{actv} \sim 0.1 - 1$ yr (following the line of reasoning above, using $f_{tot} = 0.005 - 0.02$ and $f_{orb} = 0.1 - 0.5$). If 10-meter-sized impactors are assumed to be the dominant activating population, the derived typical active lifetime is $\tau_{actv} \sim 10^4 - 10^5$ yr. The active lifetime of 133P has already been observed to be at least 10 yr, well in excess of the lifetimes implied by 0.1-meter-sized activating impactors. Meanwhile, the active lifetimes implied by 10-meter-sized activating impactors are implausibly comparable to or greater than the lifetimes estimated for classical comets from the outer solar system ($\sim 10^4$ yr; *e.g.*, Levison & Duncan, 1997) that presumably contain much more ice, spend far smaller fractions of their orbit actually actively sublimating, and have only recently been perturbed into Sun-approaching orbits. Thus, the impactor size implied by the estimated crater size on 133P (§4.4) is consistent with impactor sizes implied by HTP statistics.

4.6. Possible MBC Origin

Having derived a self-consistent model of the activation and general properties of MBC activity, however, I turn to the issue of the origin of these bodies themselves. The surface area of 133P is approximately given by $A_S = 4\pi r_a^2 = 4.5 \times 10^7$ m². If a vent with $r_v = 10$ m is created every ~ 6000 yr and the probability of impacts creating such vents is assumed to be equal over 133P's surface, one would expect the potentially volatile fraction (F_{vol}) of 133P's surface (*i.e.*, the portion not yet devolatilized by impacts) to follow the exponential decay function

$$F_{vol} = e^{-f_A t} \quad (7)$$

where the fractional devolatilization rate, f_A , can be approximated by $f_A = A_S \tau_i^{-1} (\pi r_v^2)^{-1}$, and t is the elapsed time since 133P's formation. One then finds that 133P has a surface devolatilization half-life of $t_{1/2} \sim 700$ Myr, and should have less than 10% of its surface unaffected by impacts after 2.5 Gyr, its current age if it is assumed to be an original fragment from the destruction of the Themis family parent body (§1.3).

If 133P is in fact a primordial member of the Themis family, the present-day timescale for impacts by meter-sized projectiles on still-volatile portions of its surface should be $\tau_{i,vol} = \tau_i / F_{vol} \sim 6 \times 10^4$ yr. Assuming the activity detection statistics of the HTP are correct, this longer impact timescale then implies correspondingly longer active vent lifetimes of $\tau_{actv} \sim 10^3 - 10^4$ yr. Such vent

lifetimes are not inconceivable but may be considered improbable given that they are approaching the estimated active lifetimes of much icier and better-preserved classical comets (*cf.* §4.5).

Thus, for 133P to become activated on a plausible timescale without requiring implausibly long vent lifetimes, it may need to be a secondary (or even multi-generation) fragment from a recent disruption event. It and other MBCs could be sheared-off surface fragments or interior fragments of their respective parent bodies. In either case, the ice that they contain could have previously been located at great depths in those parent bodies, preserved against both solar heating and impact devolatilization, and now only recently found in shallow subsurface reservoirs.

The conclusion that 133P could be a recently-produced fragment of a larger asteroid is supported by Nesvorný *et al.* (2008) who found that 133P may be a member of the newly-identified Beagle family (named for Themis-family asteroid (656) Beagle), which they believe formed < 50 Myr ago from the catastrophic disruption of a parent object with a diameter of $D > 20$ km. The other MBCs are not members of this new family nor are they known to be linked with any other known small families or clusters, but this does not necessarily preclude their membership in small families that have yet to be identified. Studies by Cheng (2004) and Bottke *et al.* (2005) also predict that the collisional lifetime against destruction of a $D = 4$ km asteroid should be ~ 2 Gyr, indicating that if 133P and 176P were formed in the initial Themis family fragmentation event, both should have been collisionally destroyed by the present day.

5. Summary

I describe the design, execution, and analysis of the Hawaii Trails Project survey that led to the identification of the class of main-belt comets. I note the following key points regarding the survey itself:

- In an effort to find other 133P-like comets in the main asteroid belt, 657 observations were made of 599 unique asteroids belonging to five major target categories which included the Themis, Koronis, and Veritas asteroid families, the Karin cluster (a subset of the Koronis family), and kilometer-scale, low-inclination, outer-belt asteroids, where the last category also includes all Themis family members and was formulated after the discovery of the second- and third-known MBCs to match the orbital characteristics of all three MBCs known at the time.
- One surveyed object (176P; also asteroid 118401) was found to be active by this survey, and its discovery, in conjunction with the serendipitous discoveries of 133P and P/Read, led to the identification of the new class of main-belt comets.
- There are strong observational selection effects, some intentional and some unintentional, that must be considered when interpreting the statistical implications of the HTP. Ultimately, the HTP should only be considered to be representative of the populations of objects actually surveyed. Even then, it should be noted that only one detection was made, and so the standard caveats associated with small number statistics apply.
- The true abundance and distribution of main-belt comets in the main asteroid belt may not be truly known until the data from deep all-sky survey telescopes like Pan-STARRS and LSST become available. These survey telescopes will likely find many more comets in the region of the asteroid belt where 133P, P/Read, and 176P are found, but may find comets elsewhere as well, such as where P/Garradd is found. Any MBCs discovered by these survey telescopes

will still require targeted follow-up observations by human observers in order to confirm the presence of activity and determine physical and photometric properties. Dynamical analysis of newly discovered MBCs will also be essential for determining whether they are native to the regions where they are discovered or whether they may have migrated from elsewhere.

I also make the following order-of-magnitude generalizations about the MBCs from the results of the HTP and currently available data on the currently best-characterized MBC, 133P (though the usual caveats associated with small-number statistics apply):

- HTP survey statistics imply that there could be ~ 100 currently active MBCs among the kilometer-scale, low-inclination, outer belt asteroid population. Additionally, upper limits of 150, 40, and 15 active objects among kilometer-scale members of the Koronis family, Karin cluster, and Veritas family, respectively, are found. The HTP provides no information about the prevalence of active MBCs outside these target categories. It also provides little information about the size of the population of dormant MBCs (*i.e.*, asteroids that contain subsurface ice but are currently inactive).
- The estimated size of the active area on 133P is found to correspond to an impactor approximately 1 m in size creating an active vent approximately 10 m in radius, assuming that the active area is collisionally created. This result is found to be consistent with the expected impact rate of projectiles of that size in the main belt and the cometary detection rate of the HTP.
- Assuming that meter-sized impactors are responsible for initiating MBC activity, it is estimated that kilometer-scale, low-inclination, outer-belt MBCs experience a potentially activating impact roughly every 6000 yr and remain active for approximately $10^2 - 10^3$ yr after each collisional activation.
- The estimated rate of impacts and estimated typical sizes of resulting active sites imply that 133P should become significantly devolatilized over the course of 2.5 Gyr, suggesting that it may not be a primordial member of the ~ 2.5 -Gyr-old Themis family. It is suggested instead that 133P, and possibly the other MBCs as well, are fragments of more recent disruptions.

Acknowledgements. I acknowledge support of this work through a NASA Planetary Astronomy Grant (via David Jewitt) and STFC fellowship grant ST/F011016/1. I am grateful to Richard Wainscoat, Rita Mann, Jana Pittichová, and Aaron Evans for assistance with acquiring observations, Wen-Ping Chen and Wing Ip at National Central University in Taiwan for access to Lulin Observatory, Pedro Lacerda, Alan Fitzsimmons, David Asher, and Yan Fernández for valuable discussion, and an anonymous referee for helpful comments that improved this manuscript. I also thank John Dvorak, Ian Renaud-Kim, Dave Brennen, Paul DeGroot, Dan Birchall, and Ed Sousa at the UH 2.2 m telescope, Charles Sorensen and Hien Tran at Keck, Arturo Gomez and Edgardo Cosgrove at Cerro Tololo, Ming-Hsin Chang at Lulin, Chad Trujillo, Kathy Roth, and Tony Matulis at Gemini, Miki Ishii and Alanna Garay at Subaru, and Alberto Alvarez, Patricio Ugarte, and the late Hugo Schwarz at SOAR for technical support of my observations. I thank Edward Bowell at Lowell Observatory for making `astorb.dat` freely available, and NASA grant NAG5-4741 and the Lowell Observatory endowment for providing funding for that work. I also particularly thank David Jewitt for invaluable advice and support of this work.

References

- A'Hearn, M. F., & Feldman, P. D. 1992, *Icarus*, 98, 54
- Bell, J. F. 1989, *Icarus*, 78, 426
- Binzel, R. P. 1988, *Icarus*, 73, 303
- Binzel, R. P., Xu, S., & Bus, S. J. 1993, *Icarus*, 106, 608
- Boehnhardt, H., Schulz, R., Tozzi, G. P., Rauer, H., & Sekanina, Z. 1996, *IAU Circ.* 6495
- Boehnhardt, H., Sekanina, Z., Fiedler, A., Rauer, H., Schulz, R., & Tozzi, G. 1998, *Highlights Astron.*, 11A, 23
- Bottke, W. F., Durda, D. D., Nesvorný, D., Jedicke, R., Morbidelli, A., Vokrouhlický, D., & Levison, H. F. 2005, *Icarus*, 179, 63
- Brunetto, R., Vernazza, P., Marchi, S., Birlan, M., Fulchignoni, M., Orofino, V., & Strazzulla, G. 2006, *Icarus*, 184, 327
- Carusi, A., & Valsecchi, G. B. 1982, *A&A*, 115, 327
- Cheng, A. F. 2004, *Icarus*, 169, 357
- Ciesla, F. J., & Cuzzi, J. N. 2006, *Icarus*, 181, 178
- Davis, D. R. 1999, *Icarus*, 140, 49
- Dell'Oro, A., Paolicchi, P., Cellino, A., Zappalà, V., Tanga, P., & Michel, P. 2001, *Icarus*, 153, 52
- Elst, E. W., Pizarro, O., Pollas, C., Ticha, J., Tichy, M., Moravec, Z., Offutt, W., & Marsden, B. G. 1996, *IAUC* 6496
- de Elía, G. C., & Brunini, A. 2007, *A&A*, 466, 1159
- Farinella, P., & Davis, D. R. 1992, *Icarus*, 97, 111
- Farley, K. A., Vokrouhlický, D., Bottke, W. F., & Nesvorný, D. 2006, *Nature*, 439, 295
- Fernández, J. A., Gallardo, T., & Brunini, A. 2002, *Icarus*, 159, 358
- Florczak, M., Lazzaro, D., Mothé-Diniz, T., Angeli, C. A., & Betzler, A. S. 1999, *A&AS*, 134, 463
- Garradd, G. J., Sostero, G., Camilleri, P., Guido, E., Jacques, C., & Pimentel, E. 2008, *IAU Circ.*, 8969, 1
- Gilbert, A. M., & Wiegert, P. A. 2009, *Icarus*, 201, 714
- Gradie, J., & Tedesco, E. 1982, *Science*, 216, 1405
- Grossman, J. N., Alexander, C. M. O., Wang, J., & Brearley, A. J. 2000, *Meteoritics and Planetary Science*, 35, 467
- Hodapp, K. W., *et al.* 2004, *Astronomische Nachrichten*, 325, 636
- Hook, I. M., Jørgensen, I., Allington-Smith, J. R., Davies, R. L., Metcalfe, N., Murowinski, R. G., & Crampton, D. 2004, *PASP*, 116, 425
- Hsieh, H. H., & Jewitt, D. 2005, *ApJ*, 624, 1093
- Hsieh, H. H., & Jewitt, D. 2006a, *IAU Symposium*, 229, 425
- Hsieh, H. H., & Jewitt, D. 2006b, *Science*, 312, 561
- Hsieh, H. H., Jewitt, D. C., & Fernández, Y. R. 2004, *AJ*, 127, 2997
- Hsieh, H. H., Jewitt, D., & Pittichová, J. 2006, *IAU Circ.*, 8704, 3
- Hsieh, H. H., Jewitt, D., & Fernández, Y. R. 2009a, *ApJL*, 694, 111
- Hsieh, H. H., Jewitt, D., & Ishiguro, M. 2009b, *AJ*, 137, 157
- Ipatov, S. I. & Hahn, G. J. 1997, in *Lunar and Planetary Science XXVIII*(Houston: Lunar Planet. Inst.), 619
- Ivezić, Ž., *et al.* 2002, *AJ*, 124, 2943
- Jewitt, D. 1996, *Earth Moon and Planets*, 72, 185
- Jewitt, D. C. 2002, *AJ*, 123, 1039
- Jewitt, D., Yang, B., & Haghighipour, N. 2009, *AJ*, 137, 4313
- Jones, R. L., *et al.* 2009, *Earth Moon and Planets*, 27
- Jones, T. D., Lebofsky, L. A., Lewis, J. S., & Marley, M. S. 1990, *Icarus*, 88, 172
- Keil, K. 2000, *Planet. & Space Sci.*, 48, 887
- Kinoshita, D., Chen, C.-W., Lin, H.-C., Lin, Z.-Y., Huang, K.-Y., Chang, Y.-S., & Chen, W.-P. 2005, *Chinese Journal of Astronomy and Astrophysics*, 5, 315
- Knežević, Z., & Milani, A. 2003, *A&A*, 403, 1165
- Landolt, A. U. 1992, *AJ*, 104, 340
- Lebofsky, L. A., Feierberg, M. A., Tokunaga, A. T., Larson, H. P., & Johnson, J. R. 1981, *Icarus*, 48, 453
- Lecar, M., Podolak, M., Sasselov, D., & Chiang, E. 2006, *ApJ*, 640, 1115
- Levison, H. F., & Duncan, M. J. 1997, *Icarus*, 127, 13
- Luu, J. X., & Jewitt, D. C. 1990, *AJ*, 100, 913
- Luu, J. X., & Jewitt, D. C. 1992, *Icarus*, 97, 276

- Marsden, B. G. 1996, IAU Circ. 6457
- Marzari, F., Davis, D., & Vanzani, V. 1995, Icarus, 113, 168
- Masiero, J., Jedicke, R., Ďurech, Gwyn, S., Denneau, L., & Larsen, J. 2009, Icarus, in press
- McNaught, R. H., Hawkins, M. R. S., Marsden, B. G., Bus, S. J., Bohnhardt, H., Sekanin, Z., & Offutt, W. 1996, IAU Circ. 6473
- Miyazaki, S., *et al.* 2002, PASJ, 54, 833
- Mothé-Diniz, T., Roig, F., & Carvano, J. M. 2005, Icarus, 174, 54
- Nesvorný, D., Bottke, W. F., Jr., Dones, L., & Levison, H. F. 2002, Nature, 417, 720
- Nesvorný, D., Bottke, W. F., Levison, H. F., & Dones, L. 2003, ApJ, 591, 486
- Nesvorný, D., Enke, B. L., Bottke, W. F., Durda, D. D., Asphaug, E., & Richardson, D. C. 2006, Icarus, 183, 296
- Nesvorný, D., Bottke, W. F., Vokrouhlický, D., Sykes, M., Lien, D. J., & Stansberry, J. 2008, ApJ, 679, L143
- O'Brien, D. P., Greenberg, R., & Richardson, J. E. 2006, Icarus, 183, 79
- Offutt, W., Bohnhardt, H., & Marsden, B. G. 1997, MPEC 1997-T03
- Oke, J. B., *et al.* 1995, PASP, 107, 375
- Read, M. T., Bressi, T.H., Gehrels, T., Scotti, J. V., & Christensen, E. J. 2005, IAU Circ., 8624, 1
- Rivkin, A. S., Howell, E. S., Vilas, F., & Lebofsky, L. A. 2002, Asteroids III, eds. W. F. Bottke Jr., A. Cellino, P. Paolicchi, & R. P. Binzel, (University of Arizona Press, Tucson), 235
- Roig, F., Nesvorný, D., Gil-Hutton, R., & Lazzaro, D. 2008, Icarus, 194, 125
- Sasaki, T., *et al.* 2004, ApJ, 615, L161
- Sasselov, D. D., & Lecar, M. 2000, ApJ, 528, 995
- Schorghofer, N. 2008, ApJ, 682, 697
- Schwarz, H. E., *et al.* 2004, Proc. SPIE, 5492, 564
- Scott, E. R. D., & Krot, A. N. 2005, ApJ, 623, 571
- Sekanina, Z. 1990, AJ, 100, 1293
- Sonnett, S., Jedicke, R., Masiero, J., & Kleyna, J. 2008, LPI Contributions, 1405, 8308
- Tanga, P., Cellino, A., Michel, P., Zappalà, V., Paolicchi, P., & dell'Oro, A. 1999, Icarus, 141, 65
- Tóth, I. 2000, A&A, 360, 375
- Tsiganis, K., Knežević, Z., & Varvoglis, H. 2007, Icarus, 186, 484
- Vernazza, P., Mothé-Diniz, T., Barucci, M. A., Birlan, M., Carvano, J. M., Strazzulla, G., Fulchignoni, M., & Migliorini, A. 2005, A&A, 436, 1113
- Vernazza, P., *et al.* 2006, A&A, 460, 945
- Veverka, J., *et al.* 1999, Icarus, 140, 3
- Zappalà, V., Cellino, A., Farinella, P., & Knežević, Z. 1990, AJ, 100, 2030
- Zappalà, V., Cellino, A., Farinella, P., & Milani, A. 1994, AJ, 107, 772
- Zappalà, V., Bendjoya, P., Cellino, A., Farinella, P., & Froeschle, C. 1995, Icarus, 116, 291

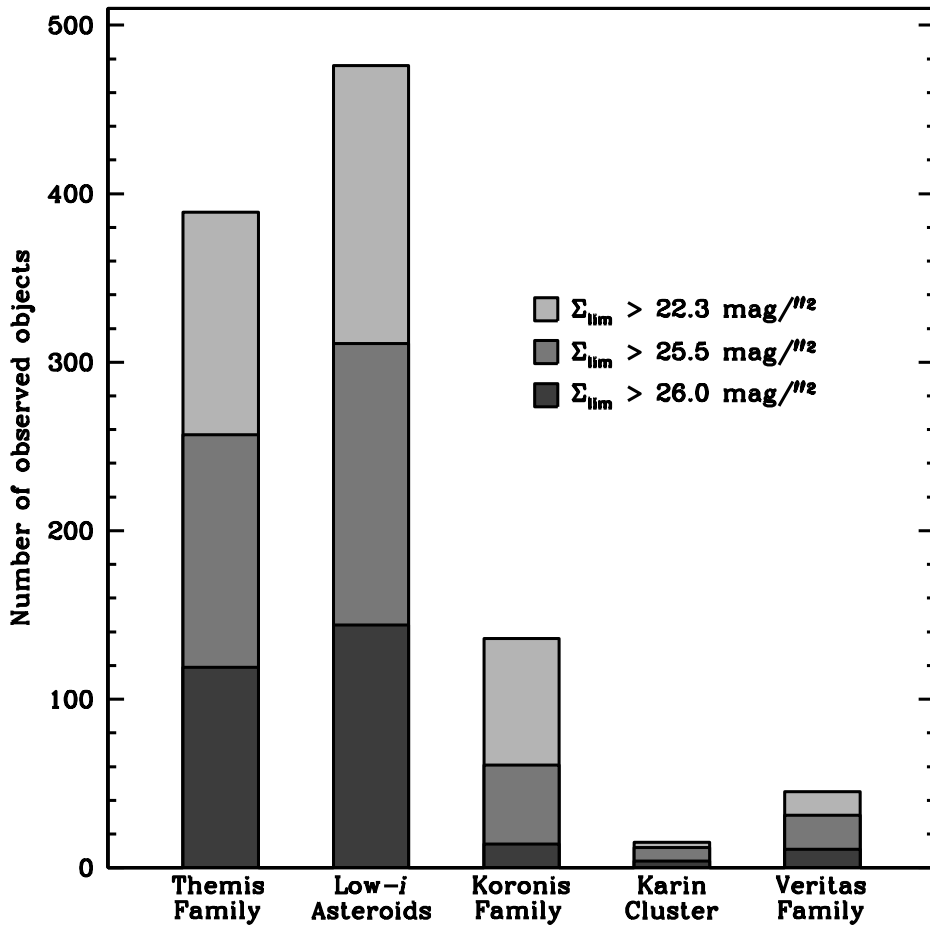


Fig. 1. Distribution of observed objects by target category, where all Themis family members are also low-inclination outer-belt asteroids, and all Karin cluster members are also Koronis family members. Observations for which activity detection limits are fainter than $22.3 \text{ mag arcsec}^{-1}$, $25.5 \text{ mag arcsec}^{-1}$, and $26.0 \text{ mag arcsec}^{-1}$ are shown in light gray, medium gray, and dark gray, respectively.

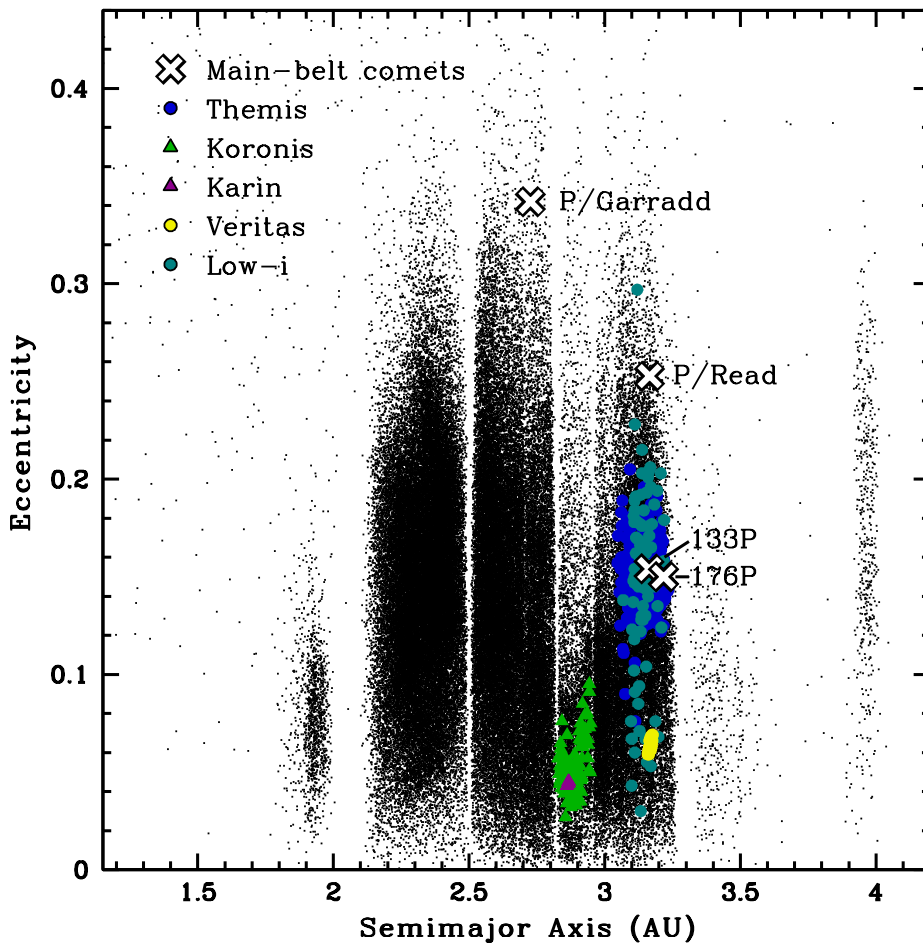


Fig. 2. Semimajor axis versus eccentricity distribution of HTP survey targets, where proper orbital elements are plotted when available and osculating orbital elements are plotted for objects for which proper orbital elements are not available. Proper orbital elements for the background main-belt asteroid population are plotted using small black dots, while orbital elements for observed HTP targets are marked as labeled. Orbital elements of the currently-known MBCs are plotted for reference, although only 176P was observed as part of this survey.

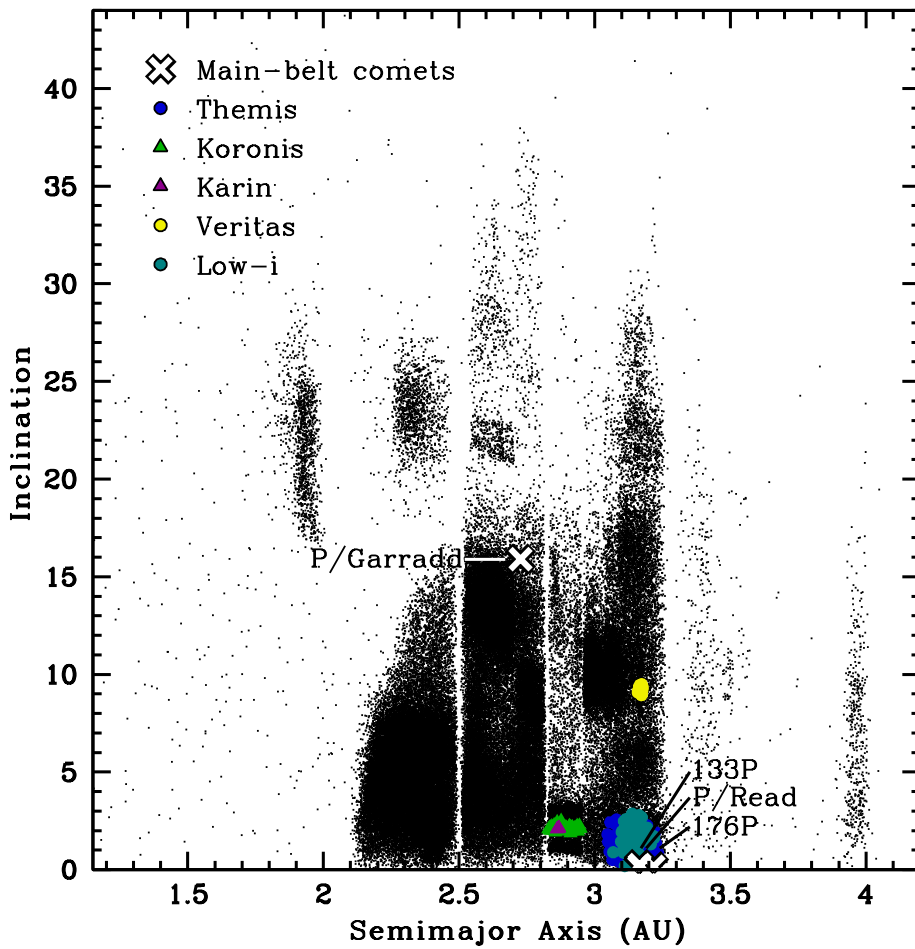


Fig. 3. Semimajor axis versus inclination distribution of HTP survey targets, where proper orbital elements are plotted when available and osculating orbital elements are plotted for objects for which proper orbital elements are not available. Proper orbital elements for the background main-belt asteroid population are plotted using small black dots, while orbital elements for observed HTP targets are marked as labeled. Orbital elements of the currently-known MBCs are plotted for reference, although only 176P was observed as part of this survey.

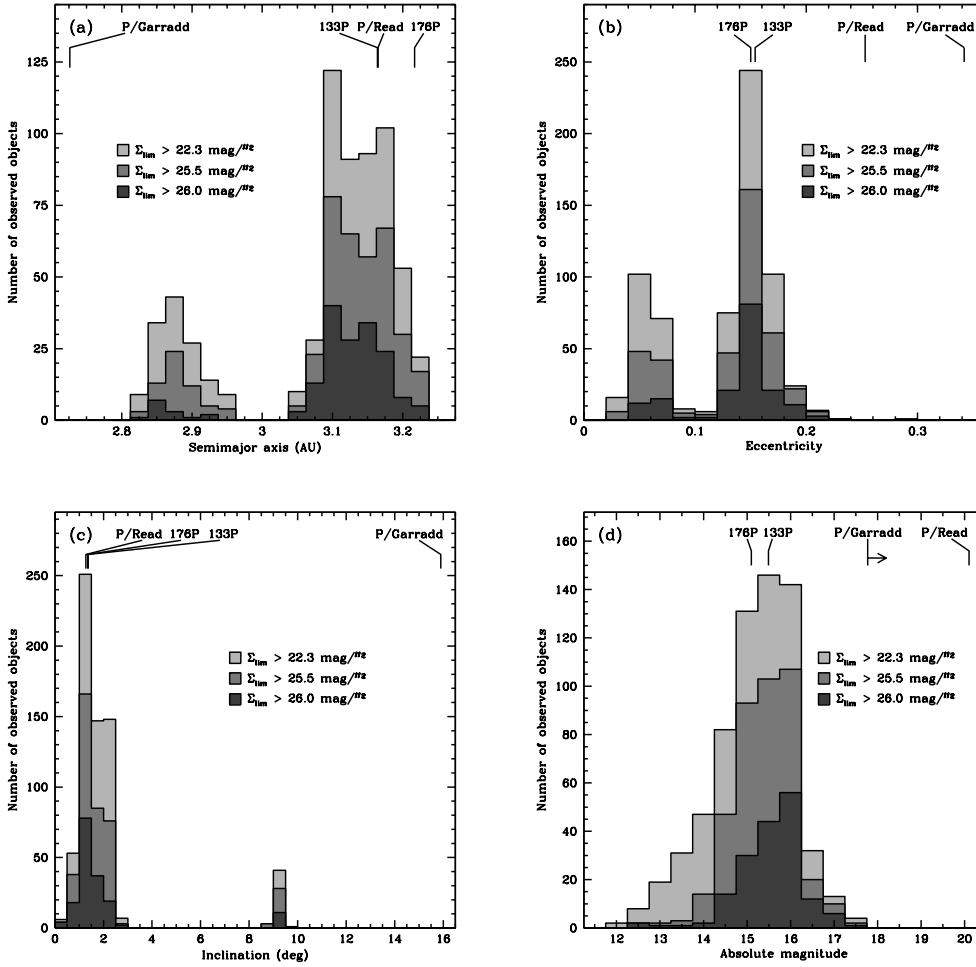


Fig. 4. Orbital and physical properties of surveyed targets, including (a) semimajor axis (a) in AU, (b) eccentricity (e), (c) inclination (i) in degrees, and (d) absolute magnitude (H_V). Proper orbital elements are used when available, while osculating orbital elements are used for objects for which proper elements are not available. Properties of the currently-known MBCs (where the absolute magnitude of P/Garradd is a lower limit) are marked for reference, although only 176P was observed as part of this survey. Observations for which activity detection limits are fainter than $22.3 \text{ mag arcsec}^{-1}$, $25.5 \text{ mag arcsec}^{-1}$, and $26.0 \text{ mag arcsec}^{-1}$ are shown in light gray, medium gray, and dark gray, respectively.

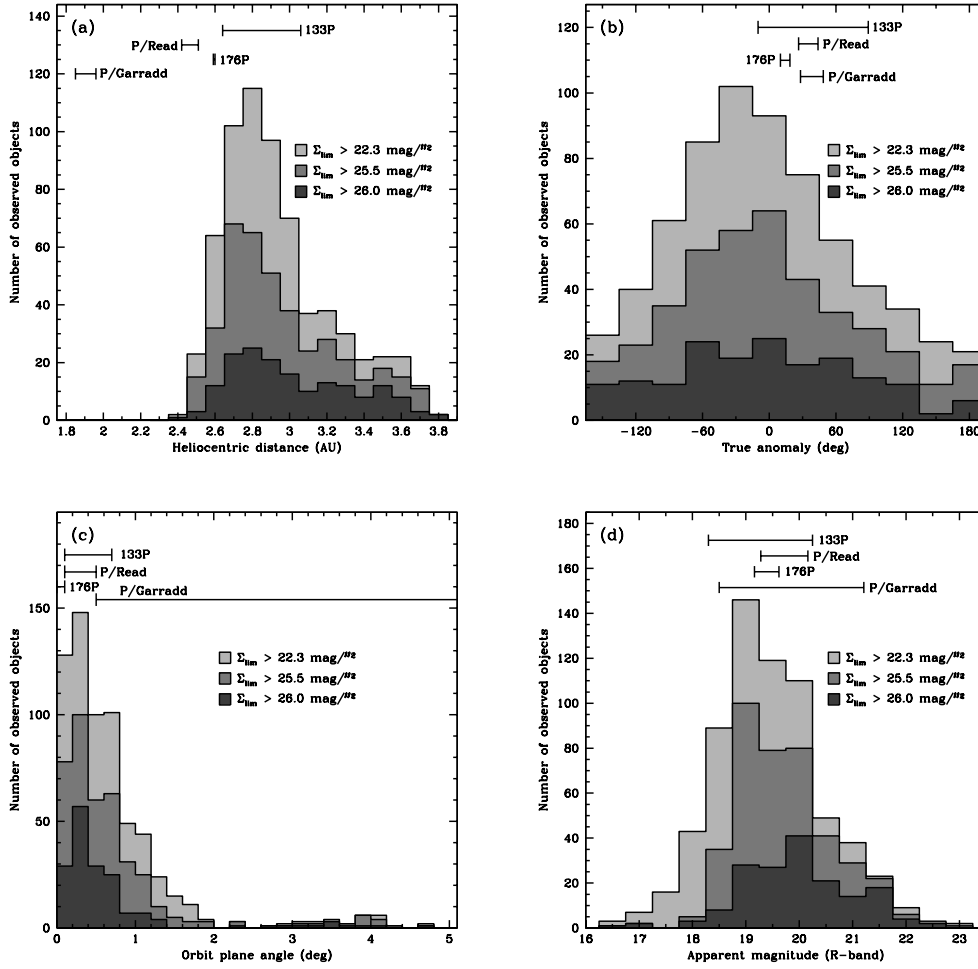


Fig. 5. Observational circumstances of surveyed targets, including (a) heliocentric distance (R) in AU, (b) true anomaly (ν) in degrees, (c) orbit plane angle (α_{pl}) in degrees, and (d) apparent R -band magnitude. The observational circumstances of the currently-known MBCs during their observed active periods are marked for reference, although only 176P was observed as part of this survey. Observations for which activity detection limits are fainter than $22.3 \text{ mag arcsec}^{-1}$, $25.5 \text{ mag arcsec}^{-1}$, and $26.0 \text{ mag arcsec}^{-1}$ are shown in light gray, medium gray, and dark gray, respectively.

Table 1. Telescope Summary

Telescope	Instrument	Pix. Scale ^a	FOV ^b	Nights	N_{obj} ^c
CTIO 1.0 m	Apogee512	0':47	4:0 × 4:0	8	67
CTIO 1.0 m	Y4KCam	0':289	19:6 × 19:6	4	24
Gemini 8.1 m	GMOS	0':146	5:5 × 5:5	1	36
Keck I 10 m	LRIS (Red)	0':210	7:2 × 7:2	2	52
Lulin 1.0 m	VA1300B	0':516	11:2 × 11:2	7	36
SOAR 4.1 m	SOI	0':154	5:3 × 5:3	4	28
Subaru 8.2 m	SuprimeCam	0':20	34' × 27'	1	47
UH 2.2 m	Optic	0':14	9:6 × 9:6	9	48
UH 2.2 m	Tek2048	0':219	7:5 × 7:5	52	319

^a Pixel scale of instrument in arcsec pixel⁻¹

^b Field of view in arcmin in the plane of the sky

^c Total number of objects observed

Table 2. Observing Run Summary

UT Date	Telescope	Instrument	Weather ¹	Moon ²	Seeing ³	n_{obj} ⁴
2003 Sep 29	UH 2.2m	Tek2048	clear	N+3	1.0	3
2003 Sep 30	UH 2.2m	Tek2048	clear	N+4	1.1	4
2003 Dec 12	UH 2.2m	Tek2048	clear	N-11	1.1	3
2003 Dec 13	UH 2.2m	Tek2048	clear	N-10	1.5	1
2004 Apr 14	UH 2.2m	OPTIC	clear	N-5	1.3	2
2004 Apr 15	UH 2.2m	OPTIC	clear	N-4	1.5	2
2004 Jul 23	UH 2.2m	OPTIC	clear	N+6	0.8	1
2004 Jul 24	UH 2.2m	OPTIC	clear	N+7	0.9	1
2004 Jul 25	UH 2.2m	OPTIC	clear	N+8	0.6	4
2004 Jul 26	UH 2.2m	OPTIC	clear	N+9	0.8	2
2004 Aug 08	UH 2.2m	OPTIC	clear	N-8	0.8	13
2004 Aug 09	UH 2.2m	OPTIC	clear	N-7	0.6	7
2004 Aug 10	UH 2.2m	OPTIC	clear	N-6	0.8	16
2004 Aug 13	UH 2.2m	Tek2048	cirrus	N-3	1.2	4
2004 Oct 14	UH 2.2m	Tek2048	cirrus	N+0	1.0	8
2004 Nov 04	UH 2.2m	Tek2048	cirrus	N-8	1.3	10
2004 Nov 05	UH 2.2m	Tek2048	cirrus	N-7	1.2	6
2004 Nov 06	UH 2.2m	Tek2048	cirrus	N-6	1.1	6
2004 Nov 07	UH 2.2m	Tek2048	cirrus	N-5	1.5	3
2005 Apr 10	UH 2.2m	Tek2048	clear	N+1	0.7	9
2005 Apr 12	UH 2.2m	Tek2048	clear	N+3	0.9	8
2005 Apr 13	UH 2.2m	Tek2048	cirrus	N+4	0.8	17
2005 Apr 17	UH 2.2m	Tek2048	clear	N+8	1.1	2
2005 Apr 30-01	CTIO 1.0m	512x512	clear	N-8	1.4	4
2005 May 01-02	CTIO 1.0m	512x512	cirrus	N-7	1.2	11
2005 May 04-05	CTIO 1.0m	512x512	cirrus	N-4	1.9	7
2005 May 06-07	CTIO 1.0m	512x512	cirrus	N-2	1.7	12
2005 May 07-08	CTIO 1.0m	512x512	cirrus	N-1	1.9	1
2005 May 08-09	CTIO 1.0m	512x512	cirrus	N+0	1.6	11
2005 May 09-10	CTIO 1.0m	512x512	cirrus	N+1	1.5	9
2005 May 10-11	CTIO 1.0m	512x512	cirrus	N+2	2.0	12
2005 May 16	UH 2.2m	Tek2048	clear	N+8	1.1	5
2005 May 27	UH 2.2m	Tek2048	clear	N-11	0.9	10
2005 May 28	UH 2.2m	Tek2048	clear	N-10	0.9	10
2005 May 29	UH 2.2m	Tek2048	cirrus	N-9	0.7	4
2005 May 30	UH 2.2m	Tek2048	cirrus	N-8	0.9	11
2005 May 31	UH 2.2m	Tek2048	cirrus	N-7	0.9	5
2005 Jun 08	Keck 10m	LRIS	cirrus	N+1	1.1	19
2005 Jul 06	UH 2.2m	Tek2048	cirrus	N+0	1.1	7

Table 2. continued.

UT Date	Telescope	Instrument	Weather	Moon	Seeing	n_{obj}
2005 Jul 07	UH 2.2m	Tek2048	clear	N+1	0.8	6
2005 Jul 09	UH 2.2m	Tek2048	clear	N+3	1.7	3
2005 Jul 10	UH 2.2m	Tek2048	clear	N+4	0.8	7
2005 Aug 25	UH 2.2m	Tek2048	clear	N-10	0.8	10
2005 Aug 26	UH 2.2m	Tek2048	clear	N-9	0.6	13
2005 Aug 27	UH 2.2m	Tek2048	clear	N-8	0.7	8
2005 Aug 28	UH 2.2m	Tek2048	clear	N-7	0.9	14
2005 Aug 29	UH 2.2m	Tek2048	clear	N-6	0.7	8
2005 Aug 30	UH 2.2m	Tek2048	cirrus	N-5	0.9	6
2005 Sep 01	UH 2.2m	Tek2048	clear	N-3	0.9	2
2005 Sep 24	UH 2.2m	Tek2048	clear	N-9	0.9	10
2005 Sep 26	UH 2.2m	Tek2048	clear	N-7	1.2	5
2005 Sep 27-28	CTIO 1.0m	Y4KCam	cirrus	N-6	1.7	5
2005 Sep 28-29	CTIO 1.0m	Y4KCam	cirrus	N-5	2.5	5
2005 Sep 29-30	CTIO 1.0m	Y4KCam	cirrus	N-4	2.3	7
2005 Sep 30-01	CTIO 1.0m	Y4KCam	cirrus	N-3	1.5	7
2005 Oct 20	Lulin 1.0m	VA1300b	cirrus	N-13	1.9	5
2005 Oct 22	Lulin 1.0m	VA1300b	cirrus	N-11	1.7	6
2005 Oct 23	Lulin 1.0m	VA1300b	cirrus	N-10	1.8	5
2005 Oct 24	Lulin 1.0m	VA1300b	cirrus	N-9	1.5	8
2005 Oct 25	Lulin 1.0m	VA1300b	cirrus	N-8	1.5	6
2005 Oct 26	Lulin 1.0m	VA1300b	cirrus	N-7	1.4	5
2005 Oct 27	Lulin 1.0m	VA1300b	cirrus	N-6	1.5	1
2005 Nov 02	UH 2.2m	Tek2048	cirrus	N+0	1.5	2
2005 Nov 03	UH 2.2m	Tek2048	cirrus	N+1	1.5	6
2005 Nov 04	UH 2.2m	Tek2048	cirrus	N+2	1.0	6
2005 Nov 05	UH 2.2m	Tek2048	cirrus	N+3	0.6	6
2005 Nov 06	UH 2.2m	Tek2048	cirrus	N+4	0.8	9
2005 Nov 07	UH 2.2m	Tek2048	cirrus	N+5	0.7	4
2005 Nov 21	UH 2.2m	Tek2048	clear	N-10	0.7	1
2005 Nov 26	Gemini 8m	GMOS	clear	N-5	0.6	36
2005 Dec 24	UH 2.2m	Tek2048	clear	N-7	1.0	11
2005 Dec 25	UH 2.2m	Tek2048	clear	N-6	0.9	7
2005 Dec 26	UH 2.2m	Tek2048	clear	N-5	1.0	8
2005 Dec 27	UH 2.2m	Tek2048	clear	N-4	0.8	6
2006 Feb 08	UH 2.2m	Tek2048	clear	N+10	0.9	2
2006 Apr 22	UH 2.2m	Tek2048	cirrus	N-6	1.1	4
2006 Apr 23	UH 2.2m	Tek2048	cirrus	N-5	0.9	9
2006 Apr 28	UH 2.2m	Tek2048	cirrus	N+0	1.0	1
2006 Apr 30	UH 2.2m	Tek2048	cirrus	N+2	0.7	2

Table 2. continued.

UT Date	Telescope	Instrument	Weather	Moon	Seeing	n_{obj}
2006 May 22	UH 2.2m	Tek2048	cirrus	N-5	0.8	2
2006 Jun 26	Subaru	SuprimeCam	cirrus	N+1	0.6	47
2006 Jul 01	UH 2.2m	Tek2048	cirrus	N+6	0.9	3
2006 Oct 17-18	SOAR	SOI	cirrus	N-4	1.3	2
2006 Oct 18-19	SOAR	SOI	clear	N-3	0.8	7
2006 Oct 19-20	SOAR	SOI	clear	N-2	1.1	4
2006 Oct 20-21	SOAR	SOI	clear	N-1	0.8	15
2006 Nov 11	UH 2.2m	Tek2048	cirrus	N-10	1.1	2
2007 Jan 27	Keck	LRIS	clear	N+8	0.9	33
Total number of objects observed						657

¹ Weather conditions at the time of observations

² Lunar phase expressed in offset from new Moon ("N") in days

³ Typical FWHM seeing in arcsec

⁴ Number of objects observed

Table 3. Properties of Objects Imaged

Object ID	Object	n^d	Type ^b	Elem. ^c	d^d	e^e	i^f	T_J^g	H^h	UT Date ⁱ	Tel. ^j	R^k	Δ^l	α^m	α_p^n	γ^o	m_R^p	σ_m^q	r^r	S/N^s	Σ_{lim}^t	C_{dl}/C_{r1}^u
20030929.01	48821 (1997 WK ₃₅)	1	Them	P	3.193	0.191	2.28	3.17	14.5	20030929	UH2.2	2.82	2.62	20.8	0.0	299.2	19.6	0.1	1500	147	25.9	0.0009
20030929.02	68899 (2002 JL ₉₅)	1	Them	P	3.091	0.146	1.48	3.21	15.3	20030929	UH2.2	2.68	1.69	3.5	0.1	45.5	19.0	0.1	1200	215	25.9	0.0011
20030929.03	69839 (1998 SJ ₁₀)	1	Them	P	3.047	0.157	1.81	3.22	15.2	20030929	UH2.2	2.61	1.61	1.0	-0.2	317.9	18.1	0.1	900	327	25.5	0.0008
20030930.01	66065 (1998 RB ₁₃)	1	Them	P	3.115	0.147	1.47	3.20	15.2	20030930	UH2.2	2.56	1.90	19.7	0.1	358.4	18.7	0.1	900	155	25.7	0.0008
20030930.02	69220 (3030 T-3)	1	Them	P	3.053	0.157	1.57	3.22	15.3	20030930	UH2.2	2.50	2.06	22.9	0.2	344.1	19.4	0.1	1200	106	25.3	0.0020
20030930.03	71552 (2000 DR ₇)	1	Them	P	3.185	0.152	1.47	3.18	15.0	20030930	UH2.2	2.80	1.86	8.3	0.1	57.5	18.4	0.1	900	316	26.0	0.0005
20030930.04	155387 (1994 AC ₉)	1	Them	P	3.165	0.152	1.09	3.18	16.0	20030930	UH2.2	2.63	1.69	9.7	0.9	332.7	19.3	0.1	1500	140	26.0	0.0014
20031212.01	47085 (1999 AW ₂)	1	Them	P	3.110	0.152	1.01	3.20	14.5	20031212	UH2.2	2.68	1.71	4.8	-0.4	44.5	17.9	0.1	600	206	25.3	0.0007
20031212.02	68451 (2001 SZ ₃₁)	2	Them	P	3.161	0.157	0.95	3.19	14.7	20031212	UH2.2	2.71	2.79	20.6	0.2	1.2	19.6	0.1	2100	83	25.9	0.0008
20031212.03	139964 (2001 SH ₇)	2	Them	P	3.095	0.144	1.10	3.21	15.0	20031212	UH2.2	2.70	2.46	21.3	0.6	18.1	20.5	0.1	2100	37	25.7	0.0025
20031213.01	112407 (2002 NU ₃₀)	1	Them	P	3.074	0.151	1.05	3.21	15.5	20031213	UH2.2	2.90	1.93	3.9	-0.4	82.5	20.1	0.1	1500	63	26.1	0.0019

* Excerpt only; full Table 3 available online at the CDS (<http://cdsweb.u-strasbg.fr/A+A.htm>)

^a Number of independent times an object was observed during the course of this survey

^b Target category of object (see § 1.3) where “Them” indicates a Themis family asteroid, “Koro” indicates a Koronis family asteroid, “Veri” indicates a Veritas family asteroid, “Kari” indicates a Karin cluster asteroid, and “Low- i ” indicates a low-inclination outer belt asteroid

^c Type of orbital elements used, where “P” indicates proper elements from the AstDyS website were used, and “O” indicates osculating elements from JPL’s Solar System Dynamics Group’s Small-Body Database (<http://ssd.jpl.nasa.gov/sbdb.cgi>) were used

^d Orbital semimajor axis in AU

^e Orbital eccentricity

^f Orbital inclination in degrees

^g Tisserand parameter, computed from listed orbital elements

^h Tisserand parameter, computed from listed orbital elements

ⁱ UT data in year, month, and day (YYYYMMDD)

^j Telescope used (CTIm: CTIO 1.0 m telescope; Gemm: Gemini North 8.1 m telescope; Keck: Keck I 10 m telescope; Keck: Keck II 10 m telescope; SOAR: Southern Astrophysical Research 4.1 m telescope; Subr: Subaru 8.2 m telescope; UH2.2: University of Hawaii 2.2 m telescope)

^k Median heliocentric distance in AU; from JPL’s Solar System Dynamics Group’s Horizons ephemeris generator (<http://ssd.jpl.nasa.gov/horizons.cgi>)

^l Median geocentric distance in AU; from JPL’s Horizons ephemeris generator

^m Solar phase angle in degrees; from JPL’s Horizons ephemeris generator

ⁿ Orbit plane angle (between the observer and object orbit plane as seen from the object) in degrees; from JPL’s Horizons ephemeris generator

^o True anomaly in degrees; from JPL’s Horizons ephemeris generator

^p Approximate mean R -band magnitude of nucleus as measured from observations

^q Estimated magnitude uncertainty, where uncertainties of 0.1 mag are assigned to observations obtained during clear conditions, and uncertainties of 0.5 mag are assigned to observations obtained with cirrus present (observing conditions listed in Table 2)

^r Total effective exposure time in seconds

^s Measured signal-to-noise ratio for composite image

^t Surface brightness detection limit for activity, in mag arcsec⁻¹, as measured in a 1 arcsec² sampling aperture

^u Fractional scattering surface area of dust with respect to the nucleus cross-section, in 10⁶ km⁻¹ at the geocentric distance of the nucleus, that is represented by Σ_{lim}

Table 4. Survey Summary

Target Category	Definition ^a	Orbital Element Ranges ^b	n_{obj} ^c	n_{obs} ^d	n_{tot} ^e
Themis family	$\delta v' = 70 \text{ m s}^{-1}$ with respect to 24 Themis	$3.04 < a < 3.27, 0.05 < e < 0.23, 0.0 < i < 3.1$	342	389	2271
Low- <i>i</i> asteroids ^f	$3.0 \text{ AU} < a < 3.3 \text{ AU}, e < 0.3, i < 3.0^\circ, H_V > 14.0$	$3.09 < a < 3.21, 0.03 < e < 0.30, 0.1 < i < 2.9$	426	476	10929
Karin cluster	$\delta v' = 10 \text{ m s}^{-1}$ with respect to 832 Karin	$2.86 < a < 2.87, 0.00 < e < 0.09, 1.0 < i < 3.2$	15	15	130
Koronis family ^g	$\delta v' = 50 \text{ m s}^{-1}$ with respect to 158 Koronis	$2.83 < a < 2.95, 0.00 < e < 0.12, 0.7 < i < 3.3$	131	136	2565
Veritas family	$\delta v' = 40 \text{ m s}^{-1}$ with respect to 490 Veritas	$3.15 < a < 3.18, 0.02 < e < 0.11, 7.9 < i < 10.6$	42	45	324
Total	599	657	13818

^a Criteria used to select target list from general asteroid population, where family and cluster members are selected using hierarchical clustering (Zappalà *et al.*, 1990, 1994) and the maximum allowable δv value, $\delta v'$, with respect to each family's or cluster's reference asteroid, is listed

^b Osculating orbital element ranges for the target samples in this survey, where semimajor axis distances are in AU and inclination values are in degrees

^c Number of unique objects observed belonging to each category

^d Number of observations of objects belonging to each category (where multiple observations of single targets are counted independently)

^e Total number of known potential targets belonging to each category (as of 2009 April 1)

^f Includes all Themis family members

^g Includes all Karin cluster members

Table 5. MBC Properties

Object ^a	a^b	e^c	i^d	T_j^e	H_R^f	$R(\text{active})^g$	$v(\text{active})^h$	$\alpha_{pl}(\text{active})^i$	$m_R(\text{active})^j$	References ^k
133P/Elst-Pizarro	3.164	0.154	1.369	3.185	15.5	2.64 – 3.06	349.9 – 89.1	0.1 – 0.7	18.3 – 20.3	1,2,3
P/2005 U1 (Read)	3.165	0.253	1.267	3.153	20.1	2.42 – 2.51	26.4 – 43.9	0.1 – 0.5	19.3 – 20.2	4,5
176P/LINEAR	3.217	0.150	1.352	3.172	15.1	2.59 – 2.60	10.1 – 18.6	0.0 – 0.1	19.2 – 19.6	3,6
P/2008 R1 (Garradd)	2.726	0.342	15.903	3.217	>17.8	1.85 – 1.96	28.2 – 48.6	0.5 – 11.3	18.5 – 21.2	7,8

^a Proper orbital elements for 133P and 176P from the AstDyS website; osculating elements for P/Read and P/Garradd from JPL's Solar System Dynamics Group's Small-Body Database

^b Semimajor axis in AU

^c Eccentricity

^d Inclination in degrees

^e Tisserand invariant, as computed from tabulated orbital elements

^f Absolute R -band magnitude

^g Range of heliocentric distances, in AU, during which activity has been observed

^h Range of true anomalies, in degrees, during which activity has been observed

ⁱ Range of orbit plane angles, in degrees, during which activity has been observed

^j Range of apparent R -band magnitudes when activity has been observed

^k (1) Elst *et al.* (1996), (2) Hsieh *et al.* (2004), (3) Hsieh *et al.* (2009a), (4) Read *et al.* (2009a), (5) Hsieh *et al.* (2005), (6) Hsieh & Jewitt (2006b), (7) Garradd *et al.* (2008), (8) Jewitt *et al.* (2009)